Nuclear Engineering and Design 278 (2014) 632–643

Contents lists available at ScienceDirect

Nuclear Engineering and Design

journal homepage: www.elsevier.com/locate/nucengdes

Evaluation of the structural integrity of the CPR1000 PWR containment under steam explosion accidents

Zhang Chunyu [a], Chen Peng [b], Zhang Juanhua [b], Lin Jiming [b], Liu Yulan [c], Zhang Shishun [b], Wang Biao [a,*]

[a] Sino-French Institute of Nuclear Engineering & Technology, Sun Yat-Sen University, Zhuhai 519082, Guangdong, China
[b] China Nuclear Power Technology Research Institute, Shenzhen 518026, Guangdong, China
[c] School of Engineering, Sun Yat-Sen University, Guangzhou 510275, Guangdong, China

HIGHLIGHTS

- Detailed three dimensional finite element model with a full consideration of the complex structures, the complex materials and the complex loadings.
- Damage to the concrete structure was calculated.
- Influence of the thermal loading on the concrete barrel was evaluated.

ARTICLE INFO

Article history:
Received 15 April 2014
Received in revised form 2 August 2014
Accepted 12 August 2014

ABSTRACT

Detailed three-dimensional finite element models were set up to study the dynamic response and the possible damage of the CPR1000 PWR containment under steam explosion accidents with a full consideration of the complex geometric structures, the complex mechanical behavior of materials and the complex blast loadings. The structural integrity of the containment and the internal structures was evaluated under five typical steam explosion scenarios. In addition, the influence of the thermal loading was investigated by setting up a thermal-mechanical coupling finite element model. It is found that under steam explosions, only a small portion of energy is transferred to the concrete containment and therefore, the influence of the explosions on the containment is insignificant. Although the internal facilities and the structures are damaged severely by the blast loadings, the damage to the containment is negligible and the structural integrity is ensured. The thermal loading has a noticeable influence on the loading-capability of the containment structure. It is shown even a pure thermal load, i.e., a 150 °C temperature variation across the containment wall, can cause some damage to the concrete containment. The damage is further deepened by a simultaneous blast loading due to a steam explosion. However, the maximum depth of the damage is small compared with the thickness of the wall and the integrity of the concrete containment is still ensured.

© 2014 Published by Elsevier B.V.

1. Introduction

In a hypothetical severe accident of core melt-down in pressurized water power plants (PWRs), the primary cooling system could fail and a very high temperature would be reached (up to 3300 K; Piluso et al., 2005). In this case, the materials of the nuclear power plant could melt to form complex mixtures called corium. When the molten corium comes into contact with the coolant water in the reactor cavity, an intense and rapid heat is transferred from the melt to the water. Considering the timescale for heat transfer is shorter than the timescale for pressure relief, this can lead to the formation of shock waves and the blast loadings may endanger the surrounding structures and even the containment building (Cizelj et al., 2006; Leskovar and Uršič, 2009). Although a steam explosion event in nuclear reactor systems is considered to be a very low probability hypothetical event, it is an important nuclear safety issue because the consequence can be catastrophic considering any direct or by-passed loss of the containment integrity can lead to radioactive material release into the environment, threatening the safety of the general public.

Since the TMI-2 accident, intensive research has been carried out to study the steam explosion process (Casadei, 1997; Corradini

* Corresponding author. Tel.: +86 0756 3668967.
E-mail address: wangbiao@mail.sysu.edu.cn (B. Wang).

http://dx.doi.org/10.1016/j.nucengdes.2014.08.019
0029-5493/© 2014 Published by Elsevier B.V.

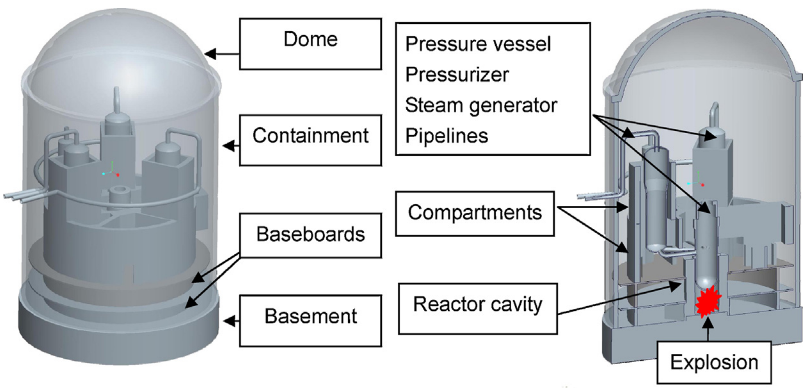

Fig. 1. Schematic of the containment and the internal components of the CPR1000 PWR.

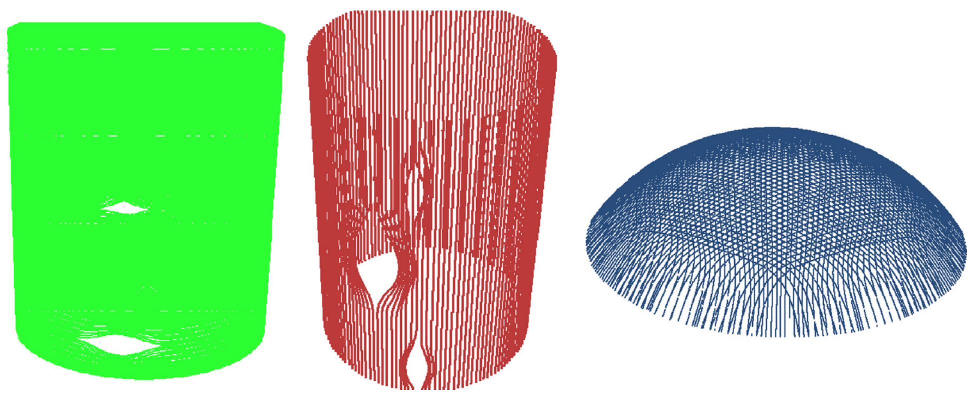

Fig. 2. Pretensioned cables of the concrete barrel (left and middle) and of the dome (right).

et al., 1988; Piluso et al., 2005; Taleyarkhan, 2005; Turland and Dobson, 1996) and several codes and models (Cizelj et al., 2006; Meignen and Picchi, 2005) have been developed to simulate different scenarios of steam explosions. Once the blast pressures due to the steam explosions are estimated, the dynamic response of the surrounding structures can be evaluated through finite element simulations. For example, the vulnerability of a partially flooded PWR reactor cavity to a steam explosion was assessed by using a stress analysis code with the pressure waves obtained by a computational fluid dynamics (CFD) code (Cizelj et al., 2006). It is worthy to note that although significant progress has been made both in steam explosion modeling and in stress analysis of complicated structures, it is still very challenging to evaluate the dynamic response and the possible damage of a PWR concrete containment under steam explosions. The challenges are not only due to the complex shock waves, but also due to the very complex geometric structures (the pressure vessel, the compartments, the reinforced concrete, the pretensioned cables, and so on) and the complex mechanical behaviors of materials (the strain rate effect, the damage and failure of concrete, the thermal-mechanical coupling) under dynamic loadings. As a consequence, quantitative assessment of the integrity of the containment under steam explosion accidents has rarely been attempted.

The aim of the present study is to evaluate the integrity of the whole containment building of the improved Chinese PWR, i.e., CPR1000, under typical scenarios of steam explosions by using numerical modeling and simulation techniques. A detailed three-dimensional finite element model is set up to study the dynamic response and the possible damage of the CPR1000 PWR containment with a full consideration of the complex geometric structures, the complex mechanical behavior of materials and the complex blast loadings. In addition to the pure mechanical loading, the influence of thermal loadings is also investigated by setting up a thermal-mechanical coupling finite element model. The deformation and the damage of each component of the whole system are calculated. The present study assesses the integrity of the whole containment structures under typical steam explosion accidents, which has rarely been reported in previous studies.

2. Modeling

2.1. Structure

The structure of the CPR1000 PWR is illustrated in Fig. 1. The height of the containment is 68 m and the radius of the dome is 24 m. The thickness of the concrete wall is 0.9 m and the thickness

Table 1
List of materials used in the CPR1000 PWR.

Components	Material	Characteristic
Concrete containment	C50 concrete	Damage, plasticity, strain rate effect
Steel rebars	HRB400 and HRB335	Plasticity, strain rate effect
Pretensioned cables	High strength steel	High strength, high tension
Steel linear	P265GH steel	Plasticity
Reactor cavity, basement, compartments	Reinforced C40 concrete	Damage, plasticity, strain rate effect
Pressure vessel and other facilities	SA508-3 steel	Moderate strain hardening, strain rate effect

Table 2
Constitutive parameters of the steel rebars.

Parameter	Value
Young's modulus (MPa)	2.0×10^5
Poisson's ratio	0.3
Density (kg/m^3)	7850
A (MPa)	400 (HPB400), 335 (HPB335)
B (MPa)	383
n	0.45
$\dot{\varepsilon}_0$	5×10^{-4}
C	0.0114
m	0.94
T_{melt} (K)	1800
T_0 (K)	293

of the steel linear is 9 mm. The thickness of the basement is 7 m. The concrete barrel is prestressed by 223 pretensioned cables in the circumferential direction and 144 pretensioned cables in the vertical direction (Fig. 2). The dome is prestressed by three groups of pretensioned cables (Fig. 2) and each group consists of 58 cables. Both the concrete barrel and the dome are heavily reinforced by steel rebars. Other concrete structures such as the compartments, the basement and the reactor cavity are reinforced as well and the reinforcement ratio is chosen according to the Chinese code for design of concrete structures (GB50010-2010).

2.2. Constitutive models

The materials used in the CPR1000 PWR and the characteristics of their mechanical behavior are listed in Table 1. The adopted constitutive model for each kind of the materials is described below.

2.2.1. Concrete

To capture the damage and failure of the concrete material, a damaged plasticity model was adopted which uses a scalar damage parameter, i.e., d, to describe the severity of the damage. $d = 0$ denotes no damage and $d = 1$ denotes complete failure. The effective elastic modulus $E = E_0\,(1 - d)$ where E_0 is the initial elastic modulus of the intact material. Verified against C30 concrete (Wang et al., 2010), a simple evolution law for the damage parameter has been proposed by Hao et al. (2012),

$$d^c = 1 - e^{-\alpha_c(\tilde{\varepsilon}_c - \varepsilon_{c0})/\varepsilon_{c0}}; \quad d^t = 1 - e^{-\alpha_t(\tilde{\varepsilon}_t - \varepsilon_{t0})/\varepsilon_{t0}} \tag{1}$$

where d^c and d^t denote the damage due to compressive deformations and tensile deformations, respectively. $\tilde{\varepsilon}_c$ and $\tilde{\varepsilon}_t$ are the inelastic compressive strain and the inelastic tensile strain, respectively. ε_{c0} and ε_{t0} are the compressive and the tensile strains at the peak compressive stress and the peak tensile stress on the complete uniaxial stress-strain curve (according to the Chinese code for design of concrete structures (GB50011-2010), $\varepsilon_{c0} = 1.59 \times 10^{-3}$ and $\varepsilon_{t0} = 1.04 \times 10^{-4}$ for C40 concrete; $\varepsilon_{c0} = 1.68 \times 10^{-3}$ and $\varepsilon_{t0} = 1.10 \times 10^{-4}$ for C50 concrete). The speed of the damage evolution is controlled by the dimensionless parameter, i.e., α_c and α_t. By default, $\alpha_c = \alpha_t = 0.5$ (Hao et al., 2012). The effective damage parameter, i.e. d, is calculated by,

$$(1 - d) = (1 - s_c d^c)(1 - s_t d^t) \tag{2}$$

where S_c and S_t are parameters describing the effect of stiffness recovery and the detailed description can be found in the documentation of the stress analysis code ABAQUS (Dassault Systèmes, 2012).

The yield function proposed by Lubliner (1989) as well as Lee and Fenves (1998) was adopted to model the yielding behavior of

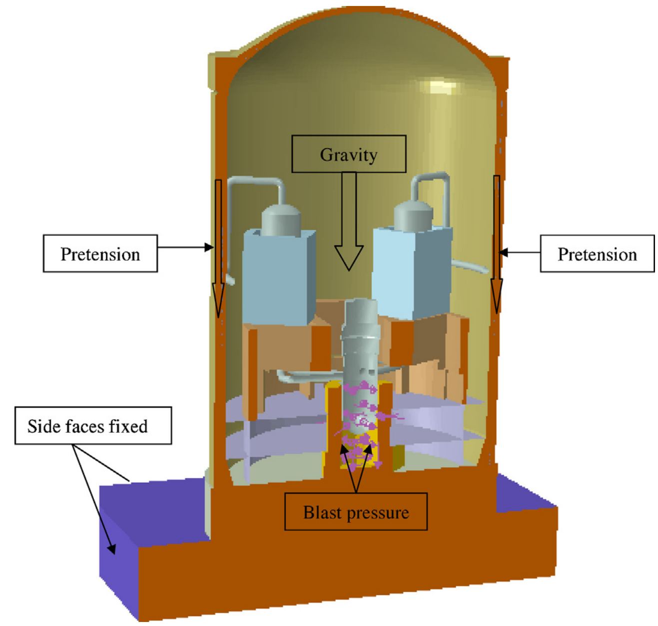

Fig. 3. Illustration of the loads and the boundary conditions.

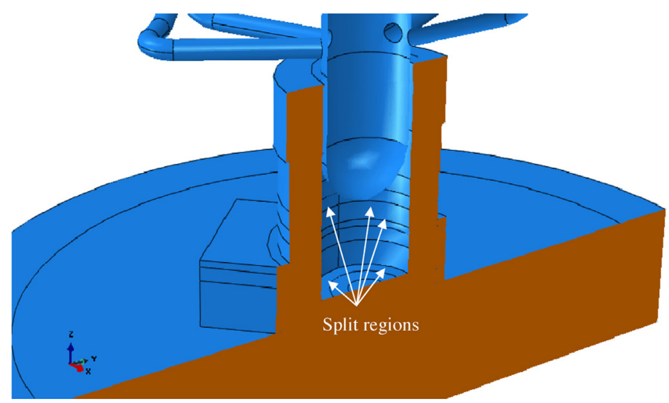

Fig. 4. Inhomogeneous pressure waves were applied on eight sub-regions.

concrete,

$$F = \frac{1}{1-\alpha}\left(\bar{q} - 3\alpha\bar{p} + \beta(\tilde{\varepsilon}^{pl})\langle\hat{\bar{\sigma}}_{\max}\rangle - \gamma\langle-\hat{\bar{\sigma}}_{\max}\rangle\right) - \bar{\sigma}_c\left(\tilde{\varepsilon}_c^{pl}\right) = 0 \tag{3}$$

where $\bar{q}$, $\bar{p}$ and $\hat{\bar{\sigma}}_{\max}$ are the von-Mises stress, the hydrostatic pressure and the maximum principal stress, respectively. $\alpha = 0.1212$; $\beta = \frac{\bar{\sigma}_y^c(\tilde{\varepsilon}^{pl})}{\bar{\sigma}_y^t(\tilde{\varepsilon}^{pl})}(1-\alpha) - (1+\alpha)$ where $\bar{\sigma}_y^c(\tilde{\varepsilon}^{pl})$ and $\bar{\sigma}_y^t(\tilde{\varepsilon}^{pl})$, respectively denote the compressive strength and the tensile strength; and $\gamma = 2.91$. The modified Prager–Drucker non-associative flow rule was adopted and the flow potential function,

$$G = \sqrt{(\ell\sigma_{t0}\tan\psi)^2 + \bar{q}^2} - \bar{p}\tan\psi \tag{4}$$

where ℓ is referred to as the eccentricity that defines the rate at which the potential function approaches the asymptote, σ_{t0} is uniaxial tensile stress at failure and ψ the dilation angle. In the present study ℓ=0.1 and $\psi = 38°$.

Both the compressive strength and the tensile strength of concrete are sensitive to strain rates (Grote et al., 2001). The strength and the compressibility increase with the strain rate. A dynamic increase factor (DIF), i.e., the ratio of the dynamics strength to the quasi-static strength, is usually used to describe the dependence of

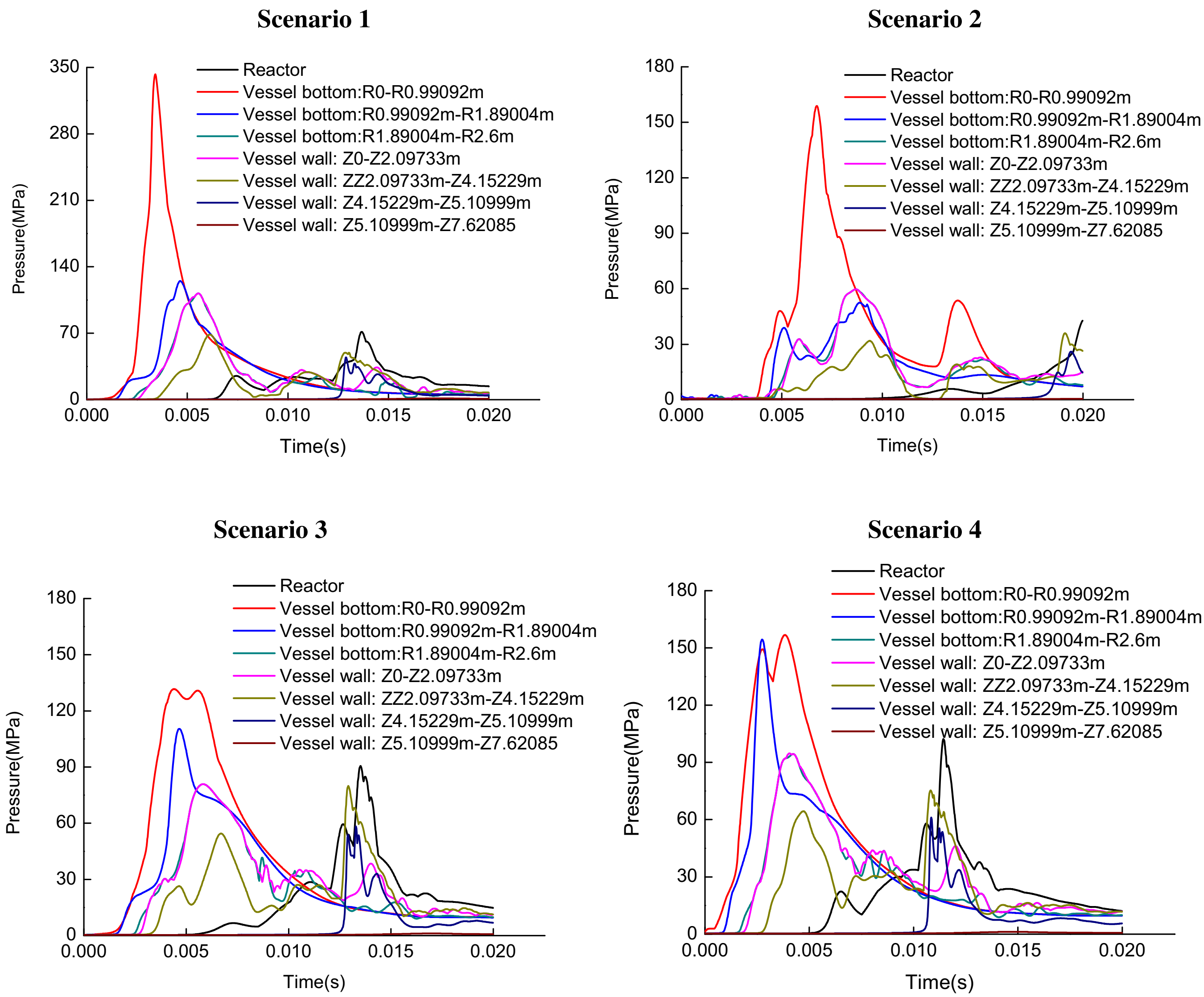

Fig. 5. The pressure waves of the typical scenarios of steam explosions.

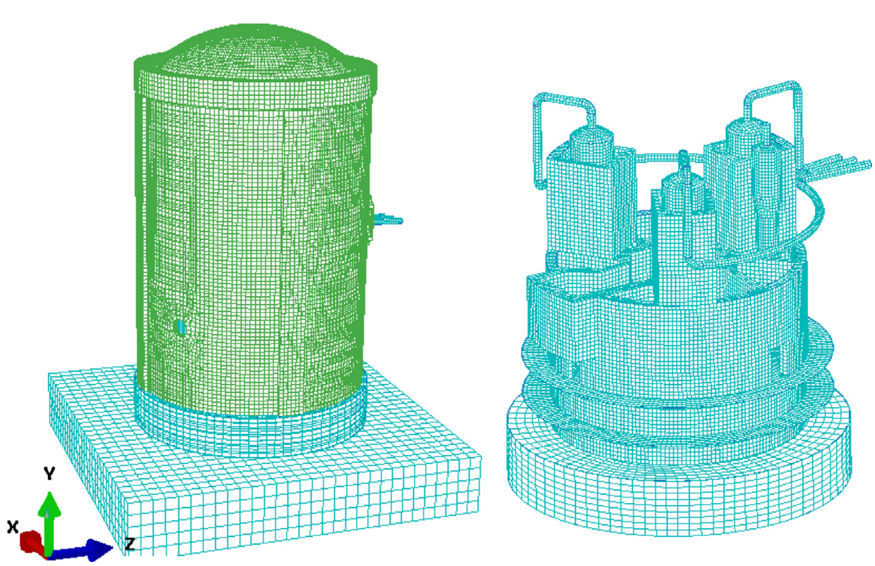

Fig. 6. Outer view (left) and inner view (right) of the finite element mesh.

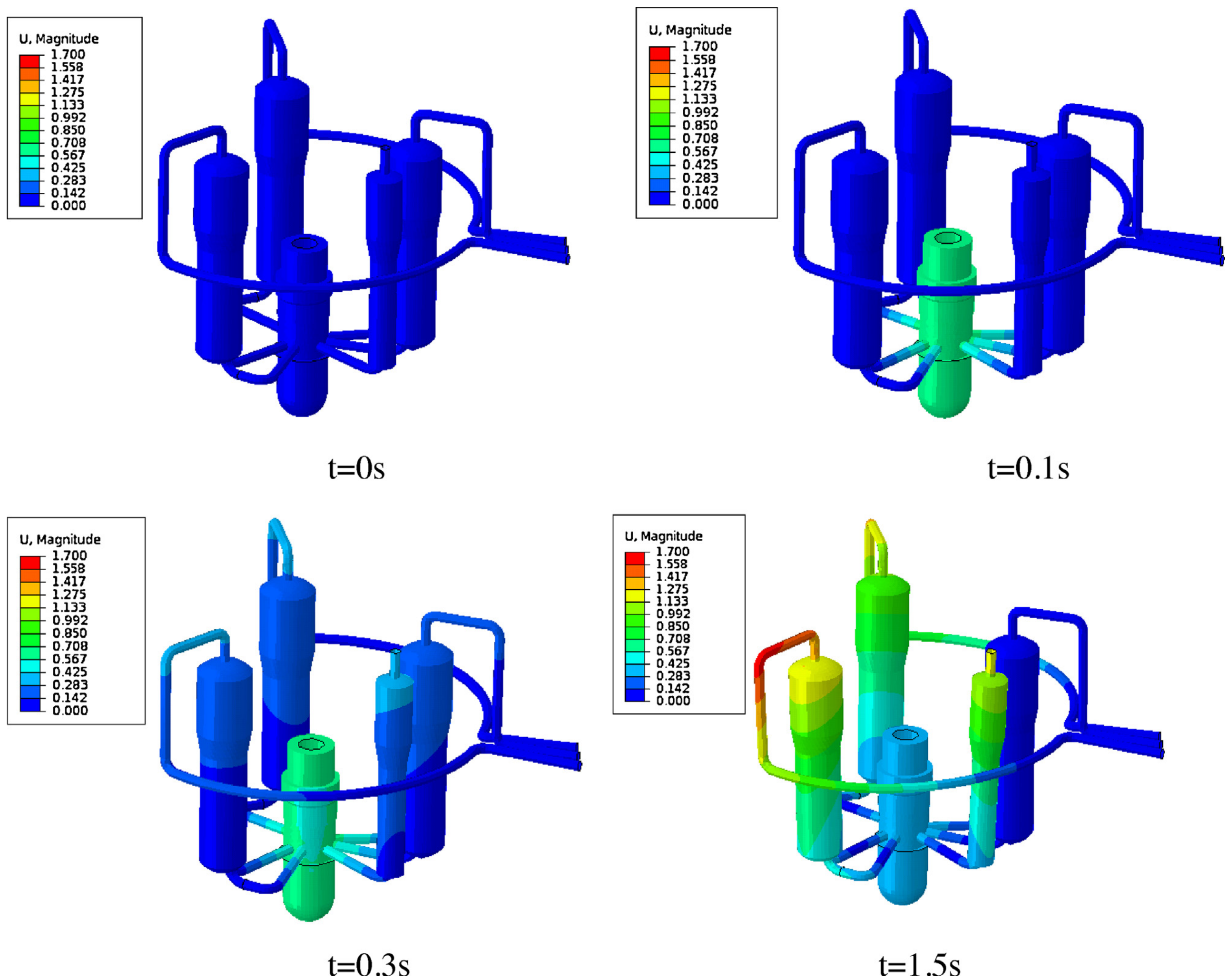

Fig. 7. Evolution of the displacements of the pressure vessel and the pipeline after the explosion. Explosion of Scenario 4 is applied.

strain rate (Tedesco et al., 1997). The master curve of DIF (Tedesco et al., 1997) was used in the present study to evaluate the dynamic strength of concrete at various strain rates.

2.2.2. Steel rebars

The classical Johnson–Cook model (Johnson and Cook, 1983, 1985) was used to describe the dependence of the yield strength on the plastic strain, the strain rate and the temperature,

$$\bar{\sigma}\left(\bar{\varepsilon}^{pl}, \dot{\bar{\varepsilon}}^{pl}, \widehat{T}\right) = [A + B(\bar{\varepsilon}^{pl})^n]\left[1 + C\ln\left(\frac{\dot{\bar{\varepsilon}}^{pl}}{\dot{\varepsilon}_0}\right)\right][1 - \widehat{T}^m] \quad (5)$$

where A is the initial quasi-static yield strength, B, C, m and n are material parameters. $\dot{\varepsilon}_0$ is a reference strain rate.

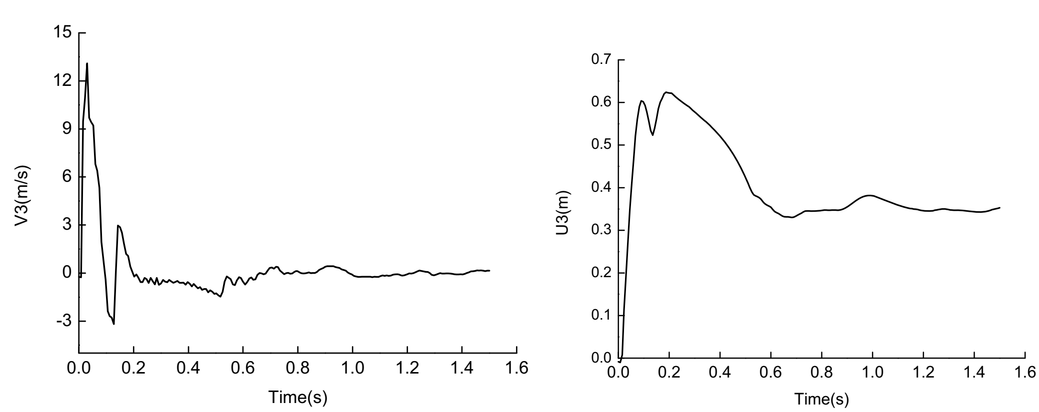

Fig. 8. Velocity and vertical displacement of one point located on the top of the pressure vessel. Explosion of Scenario 4 is applied.

Table 3
Deformations and damage of the reactor cavity and the compartments.

	Deformation and damage	Findings
Reactor cavity	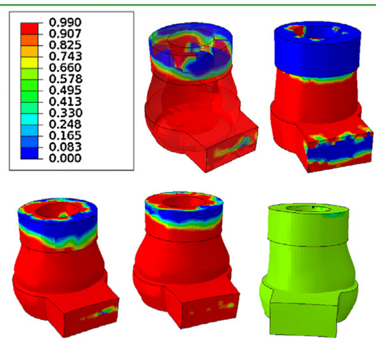	Scenarios 1-4 caused severe damages to the reactor cavity and Scenario 5 caused moderate damage to the cavity.
Base-boards	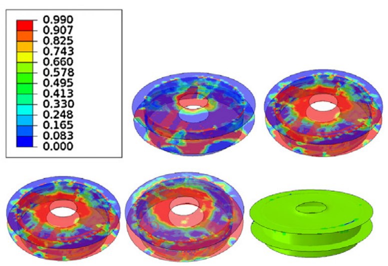	Scenarios 1-4 caused severe damages to the baseboards and Scenario 5 caused moderate damage to the baseboards.
Base-Ment (section View)	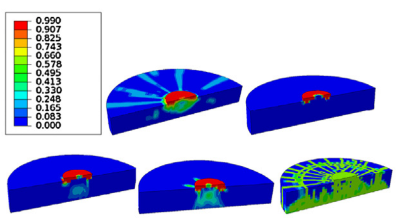	The basement was partially damaged and Scenario 4 caused the most severe damage. Parametric studies showed that a soft foundation would deteriorate the severity of damage.

$\widehat{T} = \frac{T - T_0}{T_{melt} - T_0} (T_0 \le T \le T_{melt})$ is the normalized temperature where T_0 is a reference temperature and T_{melt} is the melting point of the metal. The typical constitutive parameters of the Johnson–Cook model (Borvik et al., 2002) used in the present study are listed in Table 2.

2.2.3. *High strength steel of cables*

It is confirmed by the subsequent computations that the deformation rates of the pretensioned cables are low and therefore the strain rate effect is neglected. The yield strength is 1770 MPa and the strain hardening was assumed to be absent.

2.2.4. *P265GH steel*

It is confirmed by the subsequent computations that the deformation rate of the steel linear is low and therefore the strain rate effect is neglected. The yield strength is 320 MPa and the strain hardening was assumed to be absent.

2.2.5. *SA508-3 steel*

The mechanical property of the SA508-3 steel is sensitive to both the temperature and the strain rate. The uniaxial tensile curves at various strain rates have been measured by Sun et al. (2011) and the measured data was directly fed into the stress analysis code which automatically generated interpolated stress-strain curves if the actual strain rates were different from the fed ones.

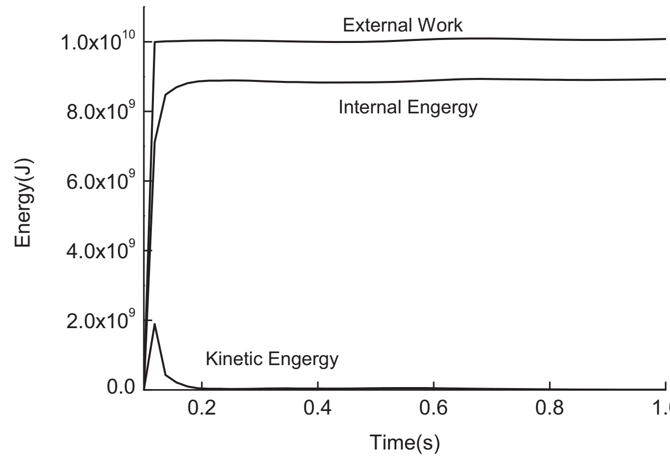

Fig. 9. Evolution of the explosion energy, the internal energy and the kinetic energy. Explosion of Scenario 4 is applied.

2.3. *Constrains, loads and boundary conditions*

A general contact was defined within the internal components and the steel linear was modeled as a shell sharing nodes with the internal surface of the concrete wall. The pretensioned cables were embedded in the solid concrete and no sliding was allowed to occur. The steel rebars were treated in a homogeneous way and an effective membrane was defined to represent each layer of the rebars. The real section area, the real space and the real orientation angle of the steel rebars were specified to calculate the section properties of the effective membranes. The effective membranes were embedded in the solid concrete and no sliding was allowed to occur. In the present study, the tightness of containment penetrations was not considered and the piping system was assumed to be coupled with the containment structures by rigid links (i.e., a kinetic coupling was defined between the pipelines and the inner surfaces of the penetration holes and therefore, the degrees of freedom the piping system are equal to the ones of the containment region within the penetration hole). The forces due to the deformation of the pressure vessel and the facilities were exerted on the concrete containment through the coupling. The rigid link may exaggerate the forces transmitted to the containment structure. The pressure vessel was supported by the reactor cavity and a contact pair was defined to model the support.

The loads and the boundary conditions of the model are illustrated in Fig. 3. Gravity was taken into account for all the components. The foundation was simplified as a thick elastic solid of which the side faces were fixed while the bottom face was free to deform. The effect of the foundation on the deformation of the basement was studied by adjusting the stiffness of the elastic solid. The loss of the pretension of the cables was calculated by the Chinese code for design of concrete structures (GB50011-2010) through the formula,

$$T = T_0 \exp(-f \cdot \alpha - \phi \cdot L) \tag{6}$$

where T is the actual pretension and T_0 is the designed pretension; f and Φ are the friction coefficients which represent the angular effect and the length effect respectively; α is the rotation angle and L is the distance of the current position with reference to the anchor of the cables. The pretension was applied by the technique of lowering the temperature of the cables element by element. Then the prestress of the concrete wall was determined by solving the equibrilium equation through the finite element method.

The pressure waves due to steam explosions were applied on the bottom surface the pressure vessel and the internal surfaces of the reactor cavity. The whole area was split into eight sub-regions

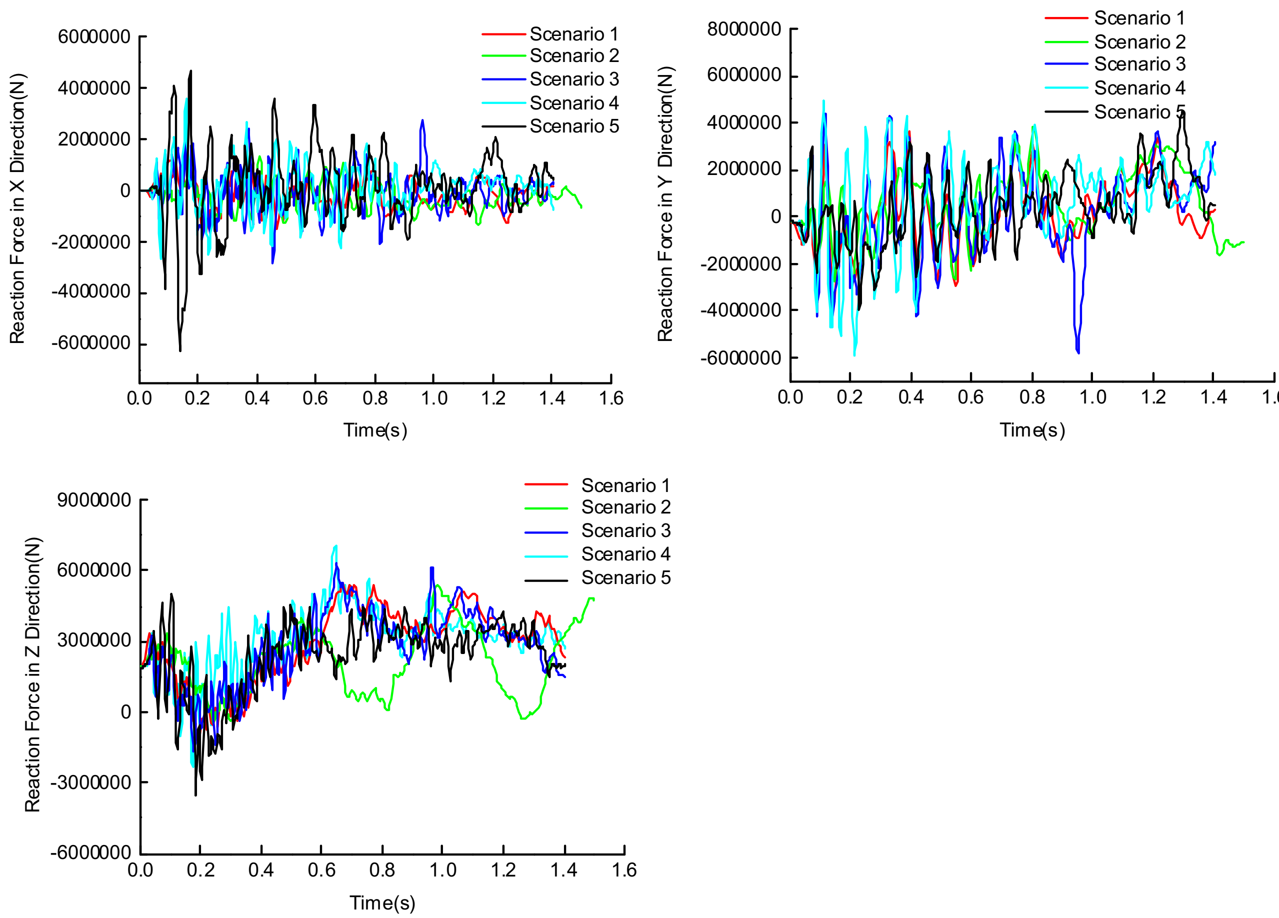

Fig. 10. Total forces transferred by the pipelines to the containment.

(Fig. 4) to facilitate the imposition of the inhomogeneous pressure waves. The bottom surface of the reactor cavity was split into three sub-regions. The radii of the cutting circles are 0.99092 m, 1.89004 m and 2.6 m. The inner wall of the reactor cavity was split into four sub-regions. The heights of the cutting plane are 2.09733 m, 4.15299 m, 5.10999 m and 7.62085 m.

Five typical scenarios of steam explosions were studied and the pressure waves were calculated by a general purpose thermo-hydraulic multiphase flow code, i.e., MC3D. It was assumed that the break area is 0.35 m^2, the initial internal pressure of the cavity is 0.3 MPa, the water level in the cavity is 3.5 m and the temperature of the corium is 2900 K. The total mass of the corium was assumed to be 155 t and 211 t, respectively, and the temperature of the water in the cavity was assumed to be 303.15 K and 373.15 K respectively. The initial conditions of the first four scenarios are set as the combination of the mass of the corium and the temperature of the cooling water in the cavity, i.e., (155 t, 303.15 K), (211 t, 303.15 K), (155 t, 373.15 K) and (211 t, 373.15 K). For the fifth scenario, the magnitude of pressure waves was same as that of the fourth scenario but the pressures were applied only on one side of each sub-region in order to roughly evaluate the effect of an inhomogeneous explosion. The pressure waves of the four typical scenarios of steam explosions were shown in Fig. 5.

2.4. Finite element mesh

Hexahedral elements (element type: C3D8R) were used to discretize the solid regions (such as the concrete wall, the basement, the reactor cavity and so on) and quadrilateral elements (element type: S4R) were used to discretize the thin-walled regions (such as the pressure vessel, the pipelines, the steel linear and so on). Membrane elements (element type: M3D4R) used to discretize the effective membranes of the steel rebars. Truss elements (element type: T3D2) were used to discretize the pretensioned cables. A point element was attached to each steam generator to account for the missing mass of the internal structures which were not included in the finite element model. Thus the weight of each steam generator was ensured to be around 510 t. The generated mesh is shown in Fig. 6. A size of round 0.3 m was chosen for all the elements to achieve a good compromise between accuracy and efficiency.

3. Results and discussion

3.1. Deformation and damage of the reactor cavity and the compartments

The deformations and the damage of the reactor cavity and the compartments caused by the five typical steam explosions are shown in Table 3. The legend illustrates the severity of damage. It is clearly shown that the Scenarios 1–4 caused severe damages to the reactor cavity and the baseboards. The concrete materials of the reactor cavity were totally destroyed while the structure did not collapse due to the support of the steel rebars. The inner regions of the baseboards were nearly destroyed while the outer regions were partially damaged. For both the cavity and the baseboards, Scenario 5 caused only moderate damage to the concrete materials because the pressures waves were applied only on one half of each sub-region in order to roughly evaluate the effect of an inhomogeneous explosion. Due to its large thickness, the basement was only partially damaged. However, preliminary parametric studies showed

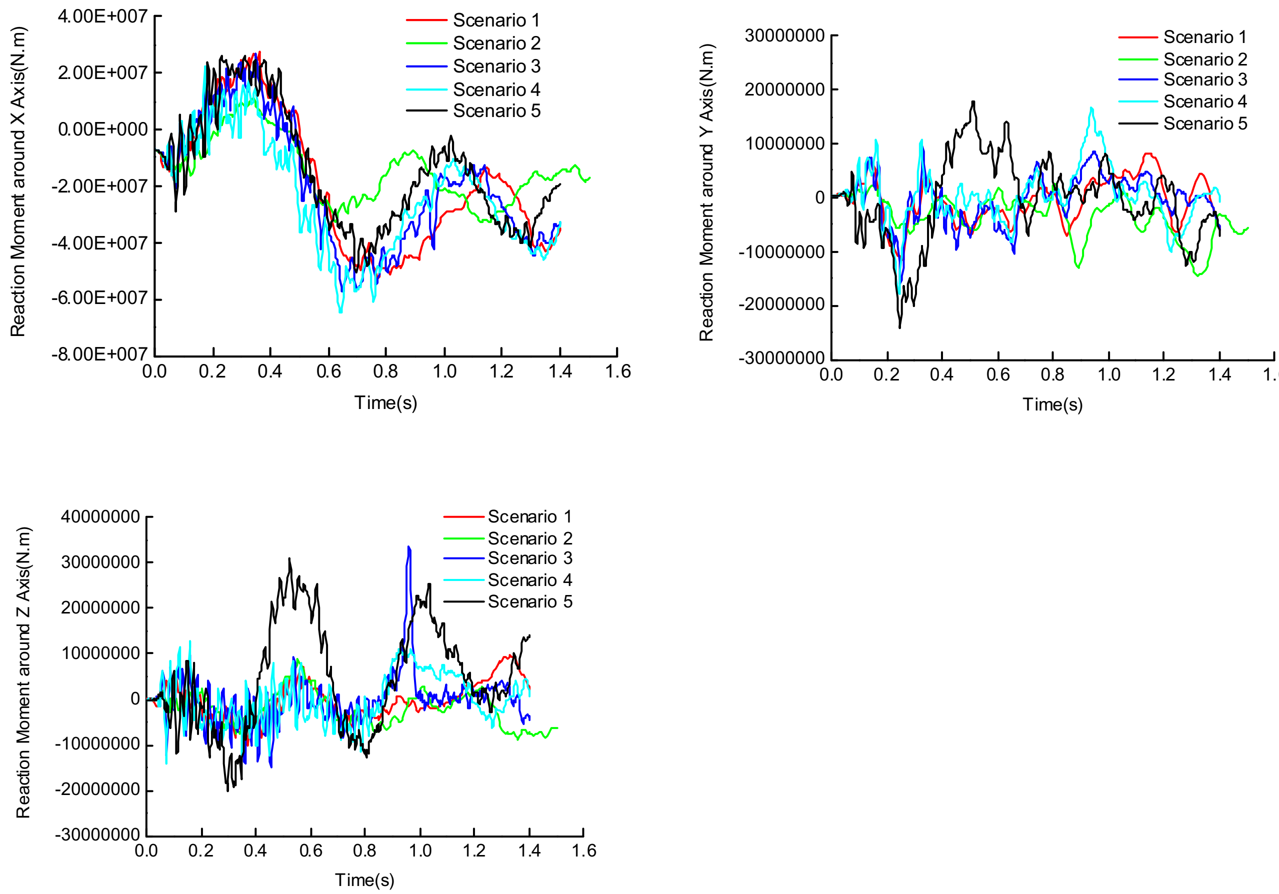

Fig. 11. Total moments transferred by the pipelines to the containment.

that the stiffness of the foundation had a noticeable influence on the damage of the basement. A hard foundation (for example, Granite) with a typical Young's modulus of 20GP and a soft foundation (for example, soil) with a typical elastic modulus of 20 MPa were compared (Lemaitre, 2001). It was found that a softer foundation deteriorated the level of the damage and in the worst case (Scenarios 4 with a soft foundation), a damage completely through the basement could be induced.

3.2. Deformation of the pressure vessel and the pipelines

Significant deformations occurred in all the scenarios among which Scenario 4 and Scenario 5 were the most dangerous. For Scenario 4, the displacements of the pressure vessel and the pipelines are shown in Fig. 7. The largest deformation was located in the pipelines and the magnitude was around 1.7 m. For Scenario 5, the magnitude of the largest deformation was around 1.5 m. Considering the total height of the pressure vessel and the pipelines is around 40 m, this deformation was not a significant one and no damage was observed in the pipelines. The deformed pipelines came into contact with the linear plates during the deformation process but they did not touch the concrete wall.

The velocity and the vertical displacement of one point located on the top of the pressure vessel are shown in Fig. 8. The velocity of the pressure vessel reached the highest around 40 ms after the explosion and the highest velocity was round 13 m/s. Around 200 ms after the explosion, the vessel reached the highest position and the vertical displacement was about 0.6 m. Obviously, the deformation process of the facilities was much slower than the explosion process which lasted only about 20 ms.

It is noticed that during the whole process of the explosions, most of the explosion energy was absorbed by the deformation of the structures and only a small fraction of the explosion energy was transferred into the kinetic energy of the structures (Fig. 9). The total forces and the moments transferred by the pipelines to the containment were shown in Fig. 10 and Fig. 11, respectively. Scenario 5 induced the largest force in *X* direction (the normal direction of the containment wall) while Scenario 4 induced the largest forces in *Y* and *Z* directions (the tangential directions of the containment wall). The largest moment in *X* direction was induced by Scenario 4 while the largest moments in *Y* and *Z* directions were induced by Scenario 5. It can be seen that the influence of Scenario 5 should nevertheless be underestimated although the pressures waves were applied only on one half of the action scope.

3.3. Deformation and damage of the concrete containment

As mentioned in Section 3.2, only a small portion of explosion energy was transferred to the concrete containment through the motion of the facilities and the damage to the concrete wall was much alleviated. The displacement of the dome under all the scenarios was no more than 26 mm. In the following, only the most dangerous Scenario 4 and Scenario 5 are analyzed.

Under Scenario 4 and Scenario 5, the moments transferred to the containment reached the highest values around 600 ms after the explosion. Only very minor damage was induced around the major hole of the containment and the depth of the damage was

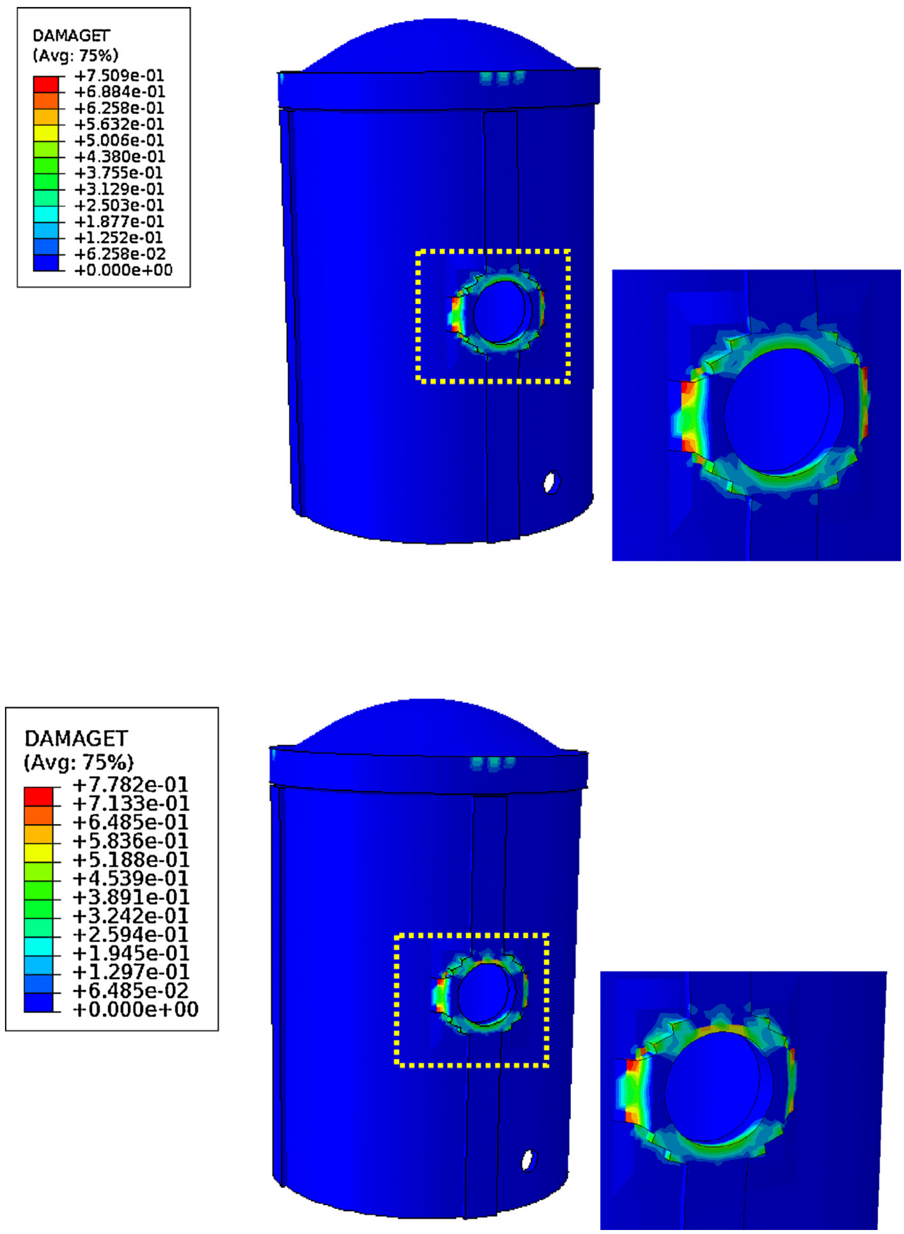

Fig. 12. Damage caused by the explosion of Scenario 4 (up) and Scenario 5 (down).

less than one fifth of the thickness of the wall (Fig. 12). The damage in other scenarios was even less. The deformation of the steel linear was very small and no damage was observed. A conclusion can be drawn that the containment remained intact under typical steam explosions.

3.4. *Influence of thermal loading*

Under severe accidents, the hot steam mixture heats up the containment and induces a temperature gradient across the containment wall. The thermal load causes not only a tensile stress to the concrete barrel of the containment but also a loss of pretension to the cables. Our previous work found that a temperature difference of 150 °C across the containment wall would cause a 15% reduction to the loading capability of the containment structure under static inner pressures. The influence of the thermal load on the structural integrity of the containment structure was also investigated in the present study and a similar technique was adopted to study the effect of the thermal loading.

A sequentially coupling thermal-mechanical finite element model was set up by extending the purely mechanical model considering the small mechanical deformation hardly influences the thermal behavior of the reactor containment. Two steps were adopted to calculate the thermal stress as well as the loss of pretension. The first step calculated the temperature distribution of the concrete containment with a temperature difference of 150 °C across the containment wall. With the calculated temperature field as the initial condition, the second step did the dynamic calculation in the same way but the pretension of the cables was modified according to their temperature. Considering the thermal conductivity of steel is much higher than that of concrete, it was assumed the influence of the cables on the temperature field of the concrete wall is insignificant and the temperature of cables was estimated through interpolating the temperature field with their positions.

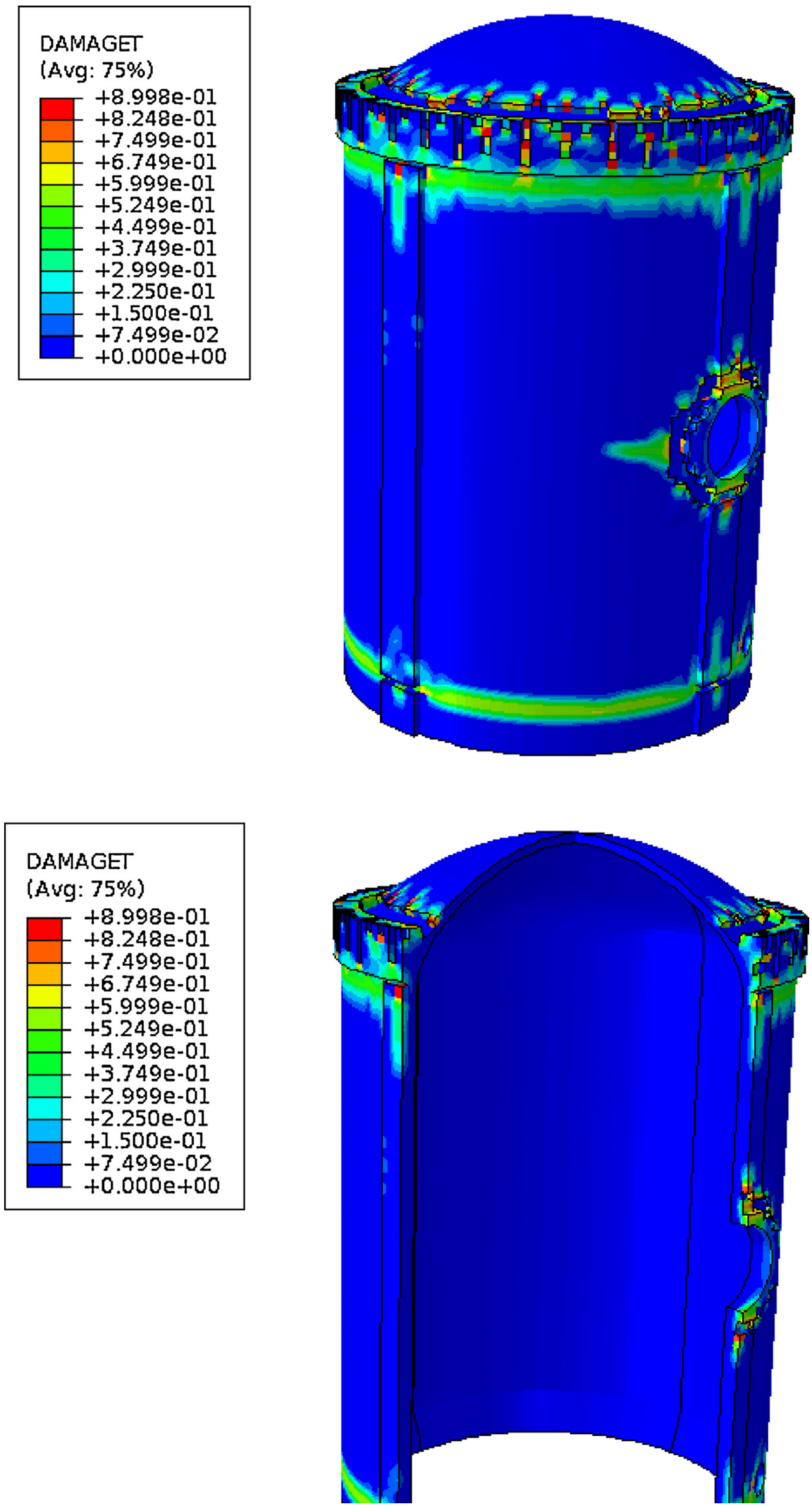

Fig. 13. Damage caused by the pure thermal load. The heavily damaged elements are hidden for clarity.

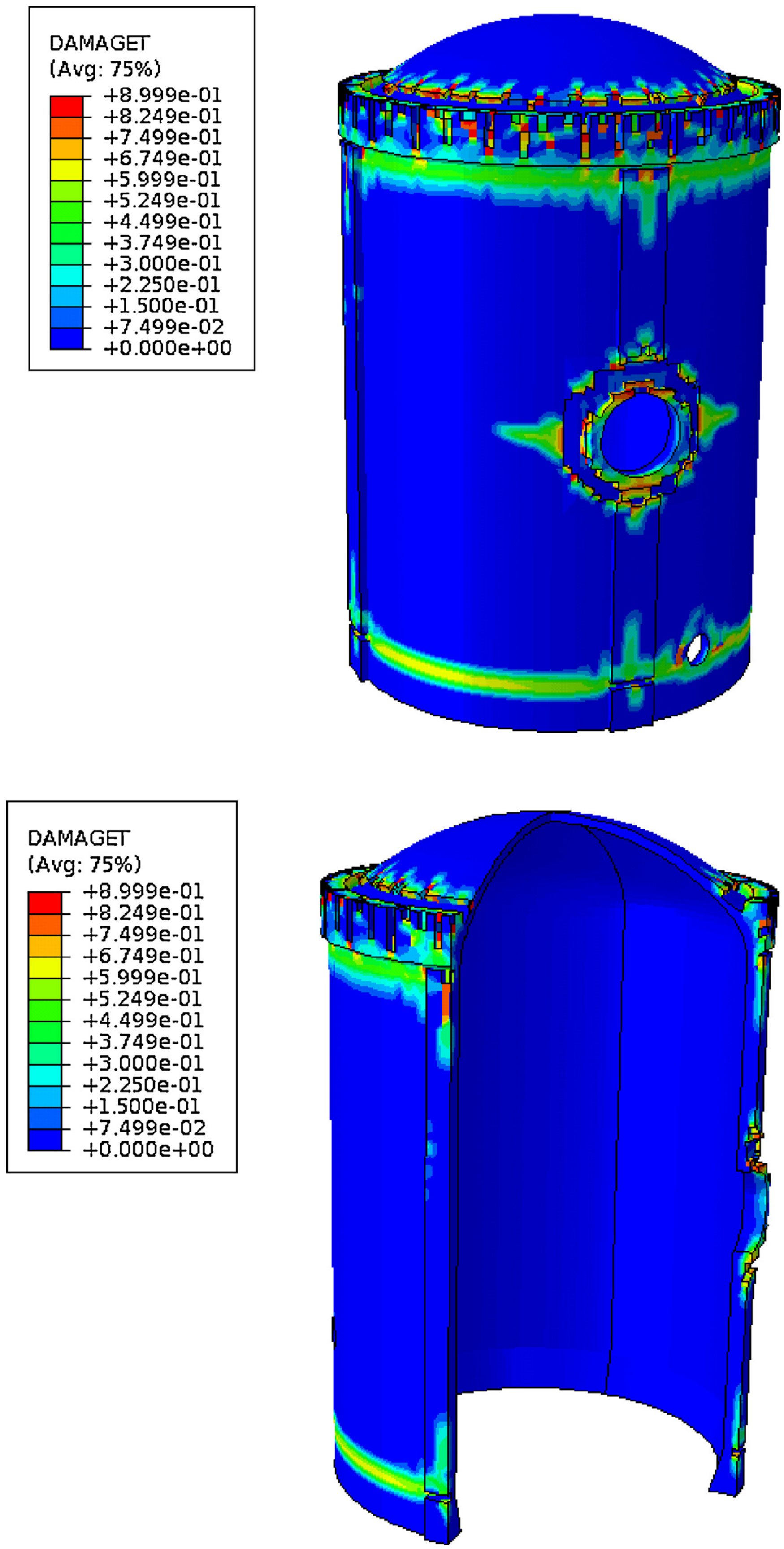

Fig. 14. Damage caused by the explosion of Scenario 4 with consideration of the thermal load. The heavily damaged elements are hidden for clarity.

It is found that some damage already occurred under a pure thermal load, i.e., a temperature difference of 150 °C across the containment wall (Fig. 13). The band-like damage located at the bottom of the dome may be due to the stress singularity considering the shafts of the cables were not modeled in the present study. The predicted position of the damaged zone is quite consistent with that reported by EDF (Electricite de France, 2013). The damage was shallow and the integrity of the containment was ensured. After the subsequent impact of the steam explosions, the damaged zones were slightly enlarged and deepened (Fig. 14). However, no penetrating damage was observed for all the scenarios of explosions and the integrity of the containment was still ensured.

4. Conclusion

Detailed three-dimensional finite element models were set up to study the dynamic response and the possible damage of the CPR1000 PWR containment under steam explosion accidents with a full consideration of the complex geometric structures, the complex mechanical behavior of materials and the complex blast loadings. It was shown that most of the blast energy was absorbed by the deformation of the facilities and the internal components. The pressure vessel and the pipelines were significantly distorted. The reactor cavity and the baseboards were severely damaged. The basement was partially damaged and it was found the stiffness of the foundation had a noticeable influence on the severity of damage. However, only a very small fraction of energy was transferred to the containment and therefore, the damage to the containment structure was much alleviated. The heating up of the containment by the steam mixture causes further damage and it is shown that a temperature difference of 150 °C across the containment wall caused even severe damages to the concrete containment. No penetrating damage was observed for all the scenarios of explosions and the integrity of the containment was ensured.

Acknowledgement

Financial support from the China Nuclear Power Technology Research Institute (CNPRI) is gratefully acknowledged.

References

Borvik, T., Hopperstad, O.S., Berstad, T., Langseth, M., 2002. Perforation of 12 mm thick steel plates by 20 mm diameter projectiles with flat, hemispherical and conical noses – Part II: Numerical simulations. Int. J. Impact Eng. 27, 37–64.
Casadei, F., 1997. Generalization of the finite element model for compressible fluids in PLEXIS-3C to multi-phase flows. Technical Note N.I. 97, 33.
GB50010-2010, 2011. Chinese Code for Design of Concrete Structures. China Architecture & Building Press, Beijing.
Cizelj, L., Končar, B., Leskovar, M., 2006. Vulnerability of a partially flooded PWR reactor cavity to a steam explosion. Nucl. Eng. Des. 236, 1617–1627.
Corradini, M.L., Kim, B.J., Oh, M.D., 1988. Vapor explosions in light water reactors. A review of theory and modelling. Prog. Nucl. Energy 22, 1–117.
Dassault Systèmes Simulia Corp., 2012. Abaqus Analysis User's Manual, V6.12.
EDF, 2013. Salome-Meca Course Materials: Overview on Civil Engineering Models. http://www.code-aster.org/V2/spip.php?article282
Grote, D.L., Park, S.W., Zhou, M., 2001. Dynamic behavior of concrete at high strain rates and pressures: I. Experimental characterization. Int. J. Impact Eng. 25, 869–886.
Hao, Y., Hao, H., Zhang, X.H., 2012. Numerical analysis of concrete material properties at high strain rate under direct tension. Int. J. Impact Eng. 39, 51–62.
Johnson, G.R., Cook, W.H.,1983. A constitutive model and data for metals subjected to large strains, high strain rates and high temperatures. In: Proceeding of the Seventh International Symposium on Ballistics. The Hague.
Johnson, G.R., Cook, W.H., 1985. Fracture characteristics of three metals subjected to various strains, strain rates, temperatures and pressures. Eng. Fract. Mech. 21, 31–48.
Lemaitre, J., 2001. Handbook of Materials Behavior Models. Academic Press, San Diego, USA.
Lee, J., Fenves, G.L., 1998. Plastic-damage model for cyclic loading of concrete structures. J. Eng. Mech. 124, 892–900.
Leskovar, M., Uršič, M., 2009. Estimation of ex-vessel steam explosion pressure loads. Nucl. Eng. Des. 239, 2444–2458.
Lubliner, J., 1989. A plastic-damage model for concrete. Int. J. Solids Struct. 25, 299–329.
Meignen, R., Picchi, S., 2005. MC3D Version 3.5: User's Guide. IRSN Report, NT/DSR/SAGR/05-84.
Piluso, P., Trillon, G., Magallon, D., 2005. Material effect and steam explosion at high temperature ($T > 2300$ K). Int. J. Thermophys. 26, 1095–1114.
Sun, M.Y., Hao, L.H., Li, S.J., Li, D.Z., Li, Y.Y., 2011. Modeling flow stress constitutive behavior of SA508-3 steel for nuclear reactor pressure vessels. J. Nucl. Mater. 418, 269–280.
Taleyarkhan, R.P., 2005. Vapor explosion studies for nuclear and non-nuclear industries. Nucl. Eng. Des. 235, 1061–1077.
Tedesco, J.W., Powell, J.C., Allen Ross, C., Hughes, M.L., 1997. A strain-rate-dependent concrete material model for ADINA. Comput. Struct. 64, 1053–1067.
Turland, B.D., Dobson, G.P., 1996. Molten Fuel Coolant Interactions: A State-of-the-art Report. EUR 16874 EN.
Wang, L.L., Zhou, F.H., Sun, Z.J., 2010. Studies on rate-dependent macro-damage evolution of materials at high strain rates. Int. J. Damage Mech. 19, 805–820.